1   **Seasonal peak photosynthesis hindered by late canopy development in northern**

2   **ecosystems**

3   Qian Zhao[1,2], Zaichun Zhu[2] ✉, Hui Zeng[2], Ranga Myneni[3], Yao Zhang[1], Josep

4   Peñuelas[4,5], Shilong Piao[1,6,7] ✉

5

6   [1] Sino-French Institute for Earth System Science, College of Urban and Environmental

7   Sciences, Peking University, Beijing 100871, China.

8   [2] School of Urban Planning and Design, Peking University, Shenzhen 518055, China.

9   [3] Department of Earth and Environment, Boston University, Boston, MA 02215, USA.

10   [4] CSIC, Global Ecology Unit CREAF-CSIC-UAB, Bellaterra 08193, Barcelona, Spain.

11   [5] CREAF, Cerdanyola del Valles 08193, Barcelona, Spain.

12   [6] Key Laboratory of Alpine Ecology, Institute of Tibetan Plateau Research, Chinese

13   Academy of Sciences, Beijing 100085, China.

14   [7] Center for Excellence in Tibetan Plateau Earth Science, Chinese Academy of Sciences,

15   Beijing 100085, China.

16

17   ✉Corresponding authors:

18   Zaichun Zhu: zhu.zaichun@pku.edu.cn

19   Shilong Piao: slpiao@pku.edu.cn

20   Manuscript for *Nature Plants*
21

22 The seasonal dynamics of the vegetation canopy strongly regulate the surface

23 energy balance and terrestrial carbon fluxes, providing feedbacks to climate

24 change. Whether the seasonal timing of maximum canopy structure was optimized

25 to achieve a maximum photosynthetic carbon uptake is still not clear due to the

26 complex interactions between abiotic and biotic factors. We used two solar-

27 induced chlorophyll fluorescence (SIF) data sets as proxies of photosynthesis, and

28 the normalized difference vegetation index (NDVI) and leaf area index (LAI)

29 products derived from the Moderate Resolution Imaging Spectroradiometer

30 (MODIS) as proxies of canopy structure, to characterize the relationship of their

31 seasonal peak timing from 2000 to 2018. We found that the seasonal peak was

32 earlier for photosynthesis than canopy structure in >87.5% of the northern

33 vegetated area, probably leading to a suboptimal maximum seasonal

34 photosynthesis. This mismatch in peak timing significantly increased during the

35 study period mainly due to the increasing atmospheric CO_2, and its spatial

36 variation was mainly explained by climatic variables (47%) and nutrient

37 limitations (28.6%). State-of-the-art ecosystem models overestimated this

38 mismatch in peak timing by simulating a delayed seasonal peak of canopy

39 development. These results highlight the importance of incorporating the

40 mechanisms of vegetation canopy dynamics to accurately predict the maximum

41 potential terrestrial uptake of carbon under global environmental change.

42

The seasonal characteristics of terrestrial vegetation strongly regulate the global carbon (C) cycle[1,2]. Changes in growing-season length (GSL) and maximum seasonal photosynthesis well explain the interannual variations of gross primary production (GPP), but maximum seasonal photosynthesis (GPP_{max}) accounts for more of the interannual changes in GPP than does GSL[3]. Understanding the underlying mechanisms that determine GPP_{max} is therefore critical[4]. The magnitude of GPP_{max} is jointly controlled by the canopy structure and the canopy performance that are regulated by environmental condition[5-8]. But the potential maximum GPP_{max} would only be achieved when the densest canopy's timing matches the timing where environmental resources are most abundant during the growing season[5,8]. In this case, the timing (day of the year, DOY) of the GPP_{max} (DOY_{GPP}) should be close to the timing of the peak canopy structure (DOY_{CAN}), i.e., synchrony of DOY_{GPP} and DOY_{CAN}. Satellite observations showed pervasive earlier DOY_{GPP} than DOY_{CAN} across the northern lands[9], indicating a "suboptimal" configuration of the seasonal canopy development. Interestingly, evidence suggests an enhancement of the peak growth of global natural vegetation[10], and an advance in DOY_{CAN} in the midlatitudes[11] and DOY_{GPP} across the north[12] in recent decades. The northern plants seem to have been adjusting the DOY_{CAN} towards a more optimal configuration for $GPP_{max,}$ but there is still room for further optimization[9]. The canopy development significantly determines the photosynthetic capacity and often consumes only a fraction of photosynthate[13]. Plants should be able to develop the densest canopy structure when the maximum seasonal resources emerge. However, why the plants across the northern lands failed to do so is unknown. The lack of an in-depth

65   understanding of the underlying mechanisms controlling the spatiotemporal variations

66   in DOY_{CAN} and its impact on GPP_{max} constitutes a large uncertainty in understanding

67   the plant's regulation mechanisms and ecosystem carbon uptake capacity under future

68   climate change.

69

70   Here, we investigate the synchrony of seasonal peak timing between photosynthesis

71   and canopy structure in northern ecosystems (>30°N) and its influencing factors during

72   2000-2018 based on satellite observations, flux tower measurements, and the boosted

73   regression tree (BRT) model that incorporates a set of 18 biotic and abiotic factors (see

74   Methods). We quantify the differences between DOY_{GPP} and DOY_{CAN} using two solar-

75   induced chlorophyll fluorescence (SIF) satellite data sets (spatially contiguous SIF,

76   CSIF[14] and SIF from the Global Ozone Monitoring Experiment-2, GOME-2 SIF[15], as

77   proxies of vegetation photosynthesis) and two vegetation indices (MODIS NDVI and

78   gap-filled MODIS LAI[16], as proxies of canopy structure). An optimized

79   "photosynthesis-canopy structure" conceptual model was built to investigate the

80   potential of maximum seasonal photosynthesis using flux-tower data (see Methods).

81   The influencing factors of the spatiotemporal differences between DOY_{GPP} and

82   DOY_{CAN} was investigated with the BRT model[17]. The performance of an ensemble of

83   fourteen state-of-the-art ecosystem models in reproducing the observed differences

84   between DOY_{GPP} and DOY_{CAN} was also evaluated.

85

86   **Results and discussion**

Seasonal peak timing and potential climatic constraints

We first analyzed the relationship of seasonal peak timing between vegetation photosynthesis, canopy structure, and climatic variables. Soil-water content (SWC) peaked across northern vegetated land in May (DOY_{SWC}: 134), followed by solar radiation (Rad) and temperature (TEMP) in June (DOY_{Rad}: 172) and July (DOY_{TEMP}: 202) respectively. Vegetation generally reaches its annual maximum photosynthesis and canopy structure in July, which is closer to the timing of the seasonal peak temperature compared to SWC and Rad. The timing of peak seasonal photosynthesis and canopy structure were mismatched, with the former peaking 8 d earlier than the latter (DOY_{CSIF}: 188 vs DOY_{NDVI}: 196) (Fig. 1a). The spatial patterns of DOY_{CSIF} and DOY_{NDVI} were nevertheless similar (Fig. 1b). Photosynthesis and canopy structure peaked around July and August at high northern latitudes and in southern China, closer to the timing of the seasonal peak of temperature, and in other temperate regions, they peaked much earlier, closer to the timing of the seasonal peak of SWC. These spatial patterns of peak timing of photosynthesis and canopy structure derived from CSIF and NDVI were also corroborated by the independent GOME-2 SIF data set and the gap-filled LAI data set (Supplementary Figs. 1-2).

Photosynthesis peaked earlier than canopy structure in >87.5% of the northern vegetated area (average negative $\delta DOY_{CSIF,\ NDVI}$ = -10 d) (Fig. 2a). The widespread negative $\delta DOY_{CSIF,\ NDVI}$ suggested that the vegetation at most northern latitudes did not allocate sufficient C to leaves to form the maximum canopy structure until the seasonal

5

109   photosynthetic peak. In contrast, 12.3% of northern vegetation (mainly in midwestern

110   Eurasia, parts of China, and midwestern North America) had a positive $\delta DOY_{CSIF, NDVI}$

111   (average positive $\delta DOY_{CSIF, NDVI}$ = 5 d), indicating a strategy prioritizing the allocation

112   of C to leaves. This relationship of peak timing between photosynthesis and canopy

113   structure was consistent with a previous study[18] and was also supported by the

114   independent GOME-2 SIF data set and the gap-filled MODIS LAI data set

115   (Supplementary Figs. 3-4). We also examined the climatic constraints on the timing of

116   seasonal peak photosynthesis across northern ecosystems based on the positioning of

117   DOY_{CSIF} with respect to the peak timing of climatic factors[12] (see Methods). We found

118   that seasonal temperature played a critical role across >75.9% of vegetated areas in

119   northern ecosystems, and water availability was the dominant factor for other regions

120   (Fig. 2b). Interestingly, the geographical distributions of $\delta DOY_{CSIF, NDVI}$ and the

121   dominant climatic constraint were strongly correlated. The temperature constraint was

122   spatially consistent with a negative $\delta DOY_{CSIF, NDVI}$, and the water constraint was

123   correlated with a positive $\delta DOY_{CSIF, NDVI}$, indicating the impacts of climatic regulation

124   on the mismatch between the peaking time of photopheresis and the canopy. In other

125   words, climatic factors seem to have influences on the strategy of seasonal allocation

126   of photosynthetic C to the canopy in the northern lands.

127

128   **Climatic and nutrient limitations explain the negative $\delta DOY_{CSIF, NDVI}$**

129   We further investigated the underlying mechanisms of the prevalent earlier peak timing

130   of seasonal photosynthesis than canopy structure (negative $\delta DOY_{CSIF, NDVI}$). To do so,

131 we trained boosted regression tree (BRT) models to examine the influence of 18 biotic

132 and abiotic factors on the negative $\delta\text{DOY}_{\text{CSIF, NDVI}}$. These factors are closely associated

133 with photosynthesis and the allocation of photosynthates, including climatic factors

134 (climatic conditions and synergies), foliar economic traits, hydraulic traits, indices of

135 biodiversity, and other related factors (see Methods). The relationship of seasonal peak

136 timing between photosynthesis and canopy structure differed across vegetation types

137 (Supplementary Fig. 5), so we developed separate BRT models for northern ecosystems

138 (entire study area), forests, shrublands, and grasslands. The BRT models performed

139 reasonably well (R^2 ranging from 0.53 to 0.78) in explaining the spatial variations of

140 negative $\delta\text{DOY}_{\text{CSIF, NDVI}}$ (Supplementary Fig. 6).

141

142 Climatic factors and foliar economic traits accounted for large fractions of the spatial

143 variation in negative $\delta\text{DOY}_{\text{CSIF, NDVI}}$ in northern ecosystems, and other three plant types

144 (24.7-36.9% for climatic conditions, 11.5-21.1% for climatic synergy, and 19.3-31.6%

145 for foliar economic traits) (Fig. 3). Climatic factors strongly influenced the peak timings

146 of seasonal photosynthesis and canopy structure in three ways: supplying solar

147 radiation, regulating light use efficiency (LUE), and determining the strategy for

148 allocating photosynthates. An obvious limitation of light was first detected at high

149 northern latitudes, with a relative contribution of radiation of 22.7% in shrublands (Rad

150 13.1% and $\delta\text{DOY}_{\text{CSIF, Rad}}$ 9.6%). We further emphasize that a decrease in radiation after

151 summer solstice may not support ongoing vegetation photosynthesis and may therefore

152 alter the seasonal synergy between photosynthesis and canopy structure, consistent with

153   a recent study reporting a limitation of light on autumnal photosynthesis[19]. LUE is

154   sensitive to environmental conditions, as predicted by many LUE models[20]. Climatic

155   synergistic variables would have obvious relative contributions if climatic factors

156   significantly accounted for the negative $\delta DOY_{CSIF, NDVI}$ by inhibiting LUE. However,

157   this was not supported due to the low contributions of $\delta DOY_{CSIF, TEMP}$ and $\delta DOY_{CSIF,}$

158    $_{SWC}$. The apparent contribution of temperature in forests (TEMP 10.6%) and shrublands

159   (TEMP 9.3%) could therefore be partly attributed to its influence on adaptive strategies

160   of allocating photosynthates. Previous studies have reported that low temperatures

161   could increase the proportion of new C allocated to roots in forests[13,21], leading to a

162   later seasonal peak of canopy structure than photosynthesis. We nonetheless cannot

163   exclude the possibility that climatic factors contributed to the negative $\delta DOY_{CSIF, NDVI}$

164   through other physiological processes, even though their influences may not have been

165   as strong as mentioned above.

166

167   Foliar economic traits are closely associated with plant photosynthetic capacity,

168   representing plant nutritional status and amount of foliage[22]. Nitrogen concentration per

169   unit dry mass (Nm), phosphorus concentration per unit dry mass (Pm), and specific leaf

170   area (SLA) were used to account for foliar economic traits. Pm was the primary factor

171   driving the spatial variation in $\delta DOY_{CSIF, NDVI}$, explaining 16.8 and 13.5% of the

172    $\delta DOY_{CSIF, NDVI}$ for forests and northern ecosystems respectively (Fig. 3). Nutrient

173   limitations have two main physiological impacts on plant growth: primarily limiting

174   the development of leaf area and secondarily regulating photosynthesis[23]. Foliar

175 phosphorus (P) concentration plays a more important role than nitrogen (N)

176 concentration in limiting the development of leaf area[23,24], but foliar N concentration

177 has a stronger and more direct influence than P concentration in regulating

178 photosynthesis[25,26]. Our results emphasize a larger contribution of foliar P concentration

179 than N concentration (Pm 13.5% vs. Nm 6.1% for northern ecosystems), suggesting

180 that foliar properties may contribute to negative $\delta DOY_{CSIF, NDVI}$ primarily by delaying

181 canopy development. Delayed canopy structure cannot develop in parallel with

182 maximum photosynthetic activity. Nm also did not significantly contribute at high

183 northern latitudes (Nm 2.4% for shrublands), even though widespread N limitation has

184 been reported[27,28], implying that the effects of nutrient limitations on photosynthetic

185 capacity were not responsible for the seasonal mismatch between photosynthesis and

186 canopy structure.

187

188 As a structural component of genetic material, P strongly controls cell division and the

189 synthesis of enzymes. Experimental studies have reported that plants reduce the growth

190 of biomass before stored P is depleted[29]. Stoichiometry, however, cannot easily set a

191 threshold of P concentration because the growth of biomass declines before P becomes

192 limited[25]. Recent studies have paid more attention to N limitation in northern

193 ecosystems, because, as a dominant component of enzymes, N directly influences

194 photosynthetic enzymatic activity[30-32]. Our study emphasizes the neglected effect of P

195 limitation on canopy development at ecosystem scales. This restriction may result in

196 delayed canopy development and seasonal decoupling of photosynthesis and canopy

197   structure and thus influence ecosystem potential maximum photosynthesis, even though

198   it is not linearly connected to photosynthetic activity. The dominant factor driving the

199   spatial variation in negative $\delta DOY_{CSIF,\ NDVI}$ differs across plant types, partly due to

200   variations in the complexity of canopy structure and environmental conditions (Fig. 3).

201   The seasonal synergy between photosynthesis and canopy structure for forests was

202   primarily controlled by P limitation (Fig. 3a). The limitation of radiation, mainly at high

203   northern latitudes, controlled the timing of peak seasonal photosynthesis for shrublands,

204   and biodiversity was also a dominant factor as a proxy for co-variation with

205   environmental resources, or as an indicator for the ability of the ecosystem in adjusting

206   the timing of the peak canopy structure that was synthesized from the different

207   phenological responses of different species[33,34] (plant species 14.9%). The

208   accumulation of C between daytime photosynthesis and nighttime consumption by

209   respiration directly determined the seasonality of canopy structure for grasslands,

210   where the diurnal range in temperature (Tdr) was larger than for other plant types (Tdr

211   17.4%). Maximum seasonal photosynthesis was generally hindered by late canopy

212   development due to nutrient limitation and climatic regulation in northern ecosystems

213   (Fig. 3b).

214

215   **GPP_max potential under an optimized synergy between canopy and resources**

216   The degree to which maximum seasonal photosynthesis (GPP_max) would be enhanced

217   if the late development of canopy structure could be adjusted to match the most

218   abundant resources in a strategy of vegetation optimization is another critical question.

219   We therefore idealized the seasonal peak timing of canopy structure using flux-tower

220   data based on an optimized "photosynthesis-canopy structure" conceptual model. The

221   seasonality of canopy structure in this model was regulated to find an optimized peak

222   timing where environmental resources were most abundant, and then an optimized

223   GPP_{max} was reconstructed jointly by the optimized canopy structure and the most

224   abundant resources (Conceptual illustration see Supplementary Fig. 7). The difference

225   between optimized and observed GPP_{max} (δGPP_{max}) can be regarded as the potential

226   increase of ecosystem GPP_{max}. Our results indicated that canopy structure peaked later

227   than photosynthesis at >80% of the flux sites (average negative $\delta DOY_{GPP, NDVI}$ = -11 d)

228   and later than the peak of environmental resources (average negative δDOY_{NDVI} = -19

229   d), implying that more resources would be obtained with an advanced peak timing of

230   canopy structure (Fig. 4). A larger asynchrony between the peak timings of

231   photosynthesis and canopy structure ($\delta DOY_{GPP, NDVI}$) generally indicated a larger

232   potential increase of GPP_{max} (R^2 = 0.68) and a more intensive regulation of the peak

233   timing of canopy structure (δDOY_{NDVI}). We emphasize that a potential increase of

234   GPP_{max} (average δGPP_{max} = 0.17 g C m^{-2} d^{-1}) would be achieved by advancing the

235   seasonal peak timing of canopy structure (average δDOY_{NDVI} = -19 d). These results at

236   the site level imply that the prevalent earlier peak timing of seasonal photosynthesis

237   than canopy structure at northern latitudes probably led to a suboptimal maximum

238   seasonal photosynthesis.

239

240   **Ecosystem models overestimated $\delta DOY_{CSIF, NDVI}$**

241 　 We evaluated the performances of 14 dynamic global vegetation models (DGVMs) that

242 　 participated in the "Trends and drivers of the regional scale sources and sinks of carbon

243 　 dioxide" project (TRENDY version 7) in reproducing the relationship of seasonal peak

244 　 timing between photosynthesis and canopy structure using their GPP and LAI results[35].

245 　 The results indicated that all the models overestimated the number of days that

246 　 vegetation photosynthesis preceded canopy structure ($\delta DOY_{GPP, LAI}$) compared with

247 　 observations, due to a notable delayed peak timing estimation of canopy structure

248 　 (DOY_{LAI}) (Fig. 5 and Supplementary Figs. 8-9). Benefiting from the mechanistic

249 　 understanding of photosynthetic processes and the unified photosynthesis module, i.e.

250 　 Farquhar model or its variants[36], the DGVMs simulated a reasonable peak timing of

251 　 photosynthesis (Supplementary Fig. 10). However, the simulation of the seasonal

252 　 dynamics of canopy structure involved processes that are currently poorly understood

253 　 and represented, especially the seasonal C allocation mechanisms, resulting in reported

254 　 systematic bias of modeled seasonal variations in LAI[37,38].

255 　 The modules of C allocation in recent DGVMs are mainly developed based on three

256 　 strategies: (1) allometric relationships between plant organs[39,40], (2) the limitation of

257 　 resources on vegetation growth[41], and (3) both allometric relationships and resource

258 　 limitation[42,43]. We divided the TRENDY models into three groups according to their

259 　 strategies for C allocation. We found that models developed based on a single C

260 　 allocation strategy provided better (but still poor) simulations of the peak timings of

261 　 canopy structure (DOY_{LAI} from 195 to 230 d for allometric relationships and DOY_{LAI}

262 $= 213$ d for resource limitation) compared with observations ($\mathrm{DOY_{NDVI}} = 196$ d) (Fig.

263 5). However, models considering both allometric relationships and resource limitation

264 do not improve their performance, simulated notably delayed $\mathrm{DOY_{LAI}}$ (221 to 255 d)

265 and thus overestimated the $\delta\mathrm{DOY_{GPP,\,LAI}}$ (-58 to -25 d). Our results emphasized that all

266 the C allocation mechanisms represented in current DGVMs need further

267 improvements, and combining allometric and resource limitation theories without

268 refinement does not improve the performance of the models in simulating seasonal

269 canopy dynamics.

270

271 **Increasing discrepancy between $\mathrm{DOY_{CSIF}}$ and $\mathrm{DOY_{NDVI}}$**

272 Satellite observations suggested that the discrepancy in peak timing between vegetation

273 photosynthesis and canopy structure significantly increased during 2000-2018 (0.39

274 d/decade, p $<$ 0.001). The overall increasing discrepancy between $\mathrm{DOY_{CSIF}}$ and

275 $\mathrm{DOY_{NDVI}}$ across the northern lands indicated that the northern vegetation might not be

276 able to tackle the environmental changes and sufficiently alter its seasonal foliar

277 allocation to achieve a larger $\mathrm{GPP_{max}}$. Interestingly, the spatial pattern of the trend in

278 $\delta\mathrm{DOY_{CSIF,\,NDVI}}$ was associated with the spatial pattern of climatic constraints on

279 photosynthesis, with the discrepancy increasing in temperature-limited regions and

280 decreasing in water-limited regions (Fig. 2b and Fig. 6b). However, the TRENDY

281 models failed to capture the observed trends in the discrepancy between $\mathrm{DOY_{CSIF}}$ and

282 $\mathrm{DOY_{NDVI}}$, in terms of both the overall trends across the northern lands (0.32±0.48

283 d/decade, $p = 0.20$) and the spatial pattern (Fig. 6c).

284

285   We further explored the effects of rising atmospheric CO_2 concentration and climate

286   change on the increasing discrepancy between DOY_{CSIF} and DOY_{NDVI} during 2000-

287   2017 based on the BRT model that considers temporal varying atmospheric CO_2

288   concentration and climate change (see Methods). The results indicated that the

289   increasing discrepancy was mainly due to CO_2 fertilization (0.49 d/decade), and was

290   slightly alleviated by climate change (-0.06 d/decade) (Supplementary Figs. 11-12).

291   The rising atmospheric CO_2 concentration amplified the discrepancy between DOY_{CSIF}

292   and DOY_{NDVI} across most of the northern vegetated lands (Supplementary Fig. 12),

293   likely due to a combined result of earlier DOY_{CSIF} due to the CO_2 fertilization effects

294   on photosynthesis and a relative stable DOY_{NDVI} that was likely limited by temperature

295   and nutrients and a more conservative carbon allocation strategy[27,44,45]. The increasing

296   CO_2-induced discrepancy suggested that there was room for further enhancement if the

297   northern vegetation could develop an earlier peak canopy structure, although CO_2

298   fertilization effects have been proved to enhance the GPP_{max}[10]. The effects of climate

299   change on $\delta DOY_{CSIF,\ NDVI}$ trend was relatively weak and spatially heterogenous

300   (Supplementary Fig. 12). We also explored the contributions of climate change and CO_2

301   fertilization to the changes in $\delta DOY_{GPP,\ LAI}$ based on TRENDY models. The model

302   simulations showed a positive effect of climate change (0.73±0.73 d/decade) and a

303   negative effect of CO_2 fertilization (-0.10±0.25 d/decade) with large spreads

304   (Supplementary Figs. 13-14), opposite to the results based on the BRT models.

305   Nevertheless, further studies are needed, especially field experiments designed to

14

306 investigate the underlying mechanisms controlling the changes in DOY_{GPP}, DOY_{CAN},

307 and the $\delta DOY_{GPP, CAN}$, which could provide explicit guidance to improve further the

308 processes and mechanisms that drive the variations in vegetation canopy development

309 in state-of-the-art ecosystem models.

310

311 This study used data from multiple sources and analyzed the synchrony between the

312 timings of seasonal peak photosynthesis and seasonal peak canopy structure at northern

313 latitudes. Our findings identified a widespread mismatch between the two peak timings

314 and an increasing discrepancy between them, suggesting that northern vegetation could

315 not mediate the seasonal canopy structure to match the availability of resources to

316 maximize its growth, with climatic regulation and nutrient limitation being potential

317 vital reasons. The current DGVMs generally performed poorly in identifying the

318 observed mismatch in peak timings. Incorporating the findings of this study will

319 provide new insights for improving the modeling of seasonal vegetation growth (e.g.,

320 P cycling and its effects on regulating peak vegetation growth). These mechanisms will

321 help improve our understanding and projection of the maximum potential uptake of C

322 by terrestrial vegetation under dramatic global environmental change.

323

324 **Methods**

325 **Data sets and study area.** We used the clear-sky CSIF data set with 4-d temporal and

326 0.05° spatial resolutions to derive the annual peak timing of vegetation photosynthesis

327 (DOY_{CSIF}) from 2000 to 2018 in northern ecosystems (>30°N). The CSIF data set uses

328　surface reflectance from the Moderate Resolution Imaging Spectroradiometer (MODIS)

329　Collection 6 (C6) (MCD43C1) as inputs and trains machine-learning algorithms on

330　daily SIF observations from Orbiting Carbon Observatory-2. It was demonstrated to

331　capture well the seasonal dynamics of satellite-observed SIF, which shows high

332　consistency with ecosystem GPP[46-48], and be suitable for vegetation phenology

333　retrievals as a proxy for GPP[14,19]. We used the NDVI data set from the MODIS C6

334　(MOD13C1) with 16-d temporal and 0.05° spatial resolutions to retrieve the annual

335　peak timing of vegetation canopy structure (DOY_{NDVI}) from 2000 to 2018. Continuous

336　snow cover leads to abundant missing data at high northern latitudes, so we

337　reconstructed the NDVI time series using an adaptive method of spatiotemporal tensor

338　completion based on the "pixel reliability" layer from the MOD13C1 data set to

339　improve the quality of the data[49]. We then interpolated CSIF and reconstructed NDVI

340　to daily temporal resolutions using linear interpolation. Another 16-day NDVI data set

341　with 500 m spatial resolution from the MODIS C6 (MOD13A1) was also used to extract

342　the seasonality of canopy structure around flux-tower sites.

343

344　To test the robustness of the peak timing of photosynthesis derived from CSIF, we used

345　an independent SIF data set from the Global Ozone Monitoring Experiment-2 (GOME-

346　2)[50]. The GOME-2 SIF v28 product suffered from sensor degradation and large

347　uncertainties due to low signal levels[51]. Therefore, we filtered the good quality

348　observations and derived the peak timing from the mean seasonal cycle of daily average

349　SIF during 2007-2018. We also used a reprocessed leaf area index (LAI) data set[16] to

350 characterize the peak timing of canopy structure in northern ecosystems to ensure the

351 robustness of our analyses. This LAI data was generated by reprocessing the MODIS

352 C6 LAI product with 8-d temporal and 0.05° spatial resolutions, and it performed more

353 continuously and consistently in temporal and spatial domains than MODIS LAI[16],

354 suitable for seasonal peak timing retrievals.

355

356 Surface air temperature (TEMP), shortwave radiation (Rad), and soil-water content

357 (SWC) were used in this analysis to define the climatic constraints on vegetation

358 photosynthesis in northern ecosystems. TEMP and Rad were obtained from the

359 Climatic Research Unit-National Centers for Environmental Prediction (CRU-NCEP,

360 version 9) with 6-h temporal and 0.5° spatial resolutions. The SWC data set was

361 provided by the Global Land Data Assimilation System (GLDAS, version 5)[52] with 3-

362 h temporal and 0.25° spatial resolutions, and we adopted SWC to a depth of 40 cm.

363 These data were aggregated into daily temporal and 0.5° spatial resolutions to derive

364 their annual peak timings (DOY_{TEMP}, $DOY_{Rad,}$ and DOY_{SWC}) from 2000 to 2018.

365

366 We used the FLUXNET2015 Tier 1 data set to analyze the potential increase of GPP_{max}

367 from the regulation of the seasonality of canopy structure. We first rigorously selected

368 sites and focused on the sites with only one seasonal GPP peak from spring to autumn

369 (52 sites, Supplementary Table 2). We controlled daily flux data with >75% valid

370 observations and calculated daily GPP as the average of both nighttime[53] and daytime[54]

371 partitioning methods. We also compared the GPP estimates of both methods and

17

372 excluded biased daily GPP to reduce the uncertainty caused by the NEE-partitioning

373 method. The observed seasonal cycles of GPP and shortwave radiation were extracted

374 from the daily data with valid fluxes.

375

376 The vegetation map was derived from the MODIS C6 (MCD12Q1) with the IGBP

377 classification scheme. We only considered vegetated areas >30°N with one peak during

378 the growing season from summer to autumn. Vegetated areas with multiple peaks

379 throughout the year were eliminated using harmonic analysis. We also ignored the

380 vegetated areas with low seasonality based on a threshold of the coefficient of variation

381 of the annual seasonal cycle of NDVI (>0.2).

382

383 **Retrieval of peak timing.** We retrieved annual peak timings of vegetation

384 photosynthesis (DOY_{CSIF}), canopy structure (DOY_{NDVI}), and climatic factors

385 (DOY_{TEMP}, DOY_{Rad}, and DOY_{SWC}) from 2000 to 2018. The peak timings were

386 identified as the days of the year when the factors arrived at their annual maxima. We

387 applied a nonparametric singular spectrum analysis (SSA) to obtain smoothed time

388 series, reduce noise, and maintain the seasonal signal of the time series[55]. SSA first

389 decomposes the original time series into oscillatory components and noises with

390 different frequencies based on the singular value decomposition and then reconstructs

391 seasonal signals using the decomposed components. This nonparametric approach can

392 reduce noise components, makes no prior assumptions about the original time series,

393 and is widely used to reconstruct time series[12,56].

394

Definition of climatic constraints. We investigated the impacts of climatic limitations on the allocation of vegetation photosynthetic carbon (C) by defining climatic constraints on vegetation growth in northern ecosystems based on the framework proposed by Park et al.[12]. This framework is based on two fundamental principles. First, vegetation photosynthesis and radiation will be seasonally consistent without climatic limitations, suggesting that DOY_{CSIF} tends to be similar to DOY_{Rad}. Second, DOY_{CSIF} will tend to be closer to the peak timing of the dominant limiting factor to obtain this more restricted resource than other factors. We adopted the idea of this framework using peak timings as proxies for resource availability. The sequential order of the peak timings of climatic factors in northern ecosystems had three scenarios: $DOY_{SWC} < DOY_{Rad} < DOY_{TEMP}$, $DOY_{Rad} < DOY_{SWC} < DOY_{TEMP}$, and $DOY_{Rad} < DOY_{TEMP} < DOY_{SWC}$ (Supplementary Fig. 15). We analyzed the climatic constraints on vegetation photosynthesis based on all three scenarios, different from the original framework only considering the most common scenario in northern ecosystems ($DOY_{SWC} < DOY_{Rad} < DOY_{TEMP}$).

Spatial analysis. We retrieved the seasonal peak timing of photosynthesis, canopy structure, and climatic variables and analyzed their multi-year average relationship from 2000 to 2018 (Fig. 1). We then quantified the mismatched peak timing between photosynthesis and canopy structure and examined the climatic constraints on the peak timing of photosynthesis (Fig. 2).

416

417 We used boosted regression tree (BRT) models to quantify the relative contributions of

418 18 extrinsic and intrinsic factors to the spatial variations of mismatched peak timing

419 between vegetation photosynthesis and canopy structure ($\delta DOY_{CSIF, NDVI}$). The BRT

420 model is a machine-learning method based on the regression tree and boosting method,

421 which can accommodate missing data and handle complex interactive effects between

422 predictors. We developed four BRT models dependent on plant type (northern

423 ecosystems, forests, shrublands, and grasslands). The BRT models were established

424 based on the "gbm" R package and defined with a tree complexity of 5, a bag fraction

425 of 0.5, and a learning rate of 0.001 or 0.01 based on the sample size of the response

426 factor. The z-scores of all numeric variables were standardized, and the response

427 variable satisfied the assumption of normality in the BRT models.

428

429 Eighteen variables were used as explanatory factors in the BRT models, including

430 climatic factors: TEMP, SWC, Rad, and diurnal temperature range (Tdr) for climatic

431 conditions and correlation coefficient between TEMP and SWC (r(TEMP, SWC)),

432 $\delta DOY_{CSIF, TEMP}$, $\delta DOY_{CSIF, SWC}$, and $\delta DOY_{CSIF, Rad}$ for climatic synergies; foliar

433 economic traits: nitrogen concentration per unit dry mass (Nm), phosphorus

434 concentration per unit dry mass (Pm), the ratio of Nm to Pm (NPr), and specific leaf

435 area (SLA); hydraulic traits: maximum rooting depth (rooting depth) and canopy height

436 (Height); indices of biodiversity: anthropogenic species richness (ASR) and plant

437 species (Species); and other related factors: GSL and tree density (Supplementary Table

438   1). The climatic factors were divided into two subcategories: climatic conditions and

439   climatic synergies, to emphasize the effects of different processes on the peak timing of

440   seasonal vegetation. Although these explanatory variables may be partially correlated,

441   the BRT model requires no prior assumption and can well handle the interactions

442   between the explanatory variables[17].

443

444   TEMP, SWC, and Rad were averaged from 2000 to 2018. Tdr was obtained from NCEP

445   v9 and averaged during the growing season of the study period to determine their effect

446   on vegetation growth. We took foliar economic traits and hydraulic traits into account

447   because they are closely associated with vegetation photosynthetic capacity and the

448   dynamics of water transport, respectively. Foliar economic traits include Nm, Pm, NPr,

449   and SLA, derived from the trait maps based on the TRY database[57]. Hydraulic traits

450   contain maximum rooting depth and canopy height obtained from the Global Earth

451   Observation project for Integrated Water Resource Assessment and the Global 1 km

452   Forest Canopy Height data set[58]. We also adopted variables of biodiversity in the BRT

453   models, including ASR and plant species, because biodiversity and ecosystem functions

454   and processes, such as terrestrial C storage and productivity, are strongly correlated.

455   ASR was developed by Ellis et al.[59] using a set of global models and estimates of

456   anthropogenic species gains and losses. Data for plant species were obtained from the

457   data set Number of Plant Species by Terrestrial Ecoregion developed by Kier et al.[60].

458   We aggregated predictive variables into a common spatial resolution of 0.5°.

459

Optimized "photosynthesis-canopy structure" conceptual model. We divided the seasonality of photosynthesis into canopy structure and environmental resources based on the light-use efficiency (LUE) – the fraction of absorbed photosynthetically active radiation (FAPAR) model framework and age-dependent LUE (Eq. 1 - 3). The seasonality of canopy structure determines the FAPAR and represents the effects of leaf age on LUE. Environmental resources represent photosynthetically active radiation (PAR) and the effects of hydrothermal conditions (HT) on LUE.

$$LUE_{(t)} = \frac{GPP_{(t)}}{PAR_{(t)} \times FAPAR_{(t)}} \qquad \text{(Eq 1)}$$

GPP was obtained from data of eddy-covariance fluxes. PAR was calculated as the product of the observed shortwave radiation from the flux-tower and 0.45. FAPAR was quantified by NDVI obtained from the MOD13A1 data set within a radius of 1 km (forests) or 200 m (grasslands and shrublands) of the flux-tower site[61], and t represents one day of the year.

$$LUE_{(t)} = HT_{(t)} \times Leaf\,Age_{(t)} \qquad \text{(Eq 2)}$$

LUE is jointly controlled by HT and Leaf Age (i.e., age-dependent LUE). Leaf Age was quantified by a linear relationship with NDVI. HT was calculated as the quotient of LUE and Leaf Age.

$$FAPAR_{(t)} \times Leaf\,Age_{(t)} = \frac{GPP_{(t)}}{PAR_{(t)} \times HT_{(t)}} \qquad \text{(Eq 3)}$$

The product of FAPAR and leaf age represents the part related to canopy structure in photosynthesis, and the product of PAR and HT indicates the effects of environmental resources on photosynthesis.

$$Optimized\ GPP_{max} = (FAPAR \times Leaf\ Age)_{max} \times (PAR \times HT)_{max} \qquad \text{(Eq 4)}$$

478   We simulated an optimized GPP_{max} assuming that the canopy structure could obtain the

479   most abundant resources by adjusting the peak timing of the canopy structure (observed

480   DOY_{NDVI}) to match the peak timing of constant seasonal environmental resources

481   (adjusted $DOY_{NDVI} = DOY_{Resources}$ and $\delta DOY_{NDVI} =$ adjusted DOY_{NDVI} - observed

482   DOY_{NDVI}). Optimized GPP_{max} could therefore be calculated as the product of seasonal

483   maximum canopy structure and seasonal maximum environmental resources.

484

485   **Model simulations.** We used GPP and LAI outputs of fourteen DGVMs from the

486   TRENDY S3 simulations (dynamic CO_2, climate, and land-use) to evaluate the

487   performances of recent DGVMs to simulate peak vegetation growth[35]. These DGVMs

488   included CABLE-POP, CLASS-CTEM, CLM5.0, DLEM, ISAM, JSBACH, JULES,

489   LPJ-GUESS, LPX, OCN, ORCHIDEE, ORCHIDEE-CNP, SURFEX, and VISIT

490   (details of individual models see Supplementary Table 3). We retrieved annual peak

491   timings of vegetation photosynthesis (DOY_{GPP}) and canopy structure (DOY_{LAI}) from

492   2000 to 2017 and calculated their difference ($\delta DOY_{GPP,\ LAI}$). Then we compared the

493   spatial patterns and temporal trends of DOY_{GPP}, DOY_{LAI}, and $\delta DOY_{GPP,\ LAI}$ with

494   observed DOY_{CSIF}, DOY_{NDVI}, and $\delta DOY_{CSIF,\ NDVI}$, respectively (Figs. 5-6 and

495   Supplementary Figs. 8-10). The model outputs from TRENDY S0-S2 simulations were

496   also used in our study and were reported in the section of temporal analysis. All model

497   outputs were linearly interpolated to a temporal resolution of 1 d and aggregated to a

498   spatial resolution of 0.5°.

499

Temporal analysis. To explore the variation in mismatched peak timing between vegetation photosynthesis and canopy structure and its potential drivers over time, we examined the trend in absolute $\delta DOY_{CSIF, NDVI}$ during 2000-2018(Fig. 6). Then, we further identified the potential drivers of the trend in $\delta DOY_{CSIF, NDVI}$ by developing a new BRT models considered temporal varying atmospheric CO_2 concentration and climatic variables. The effects of CO_2 fertilization and climate change on the trend in $\delta DOY_{CSIF, NDVI}$ can tbe attributed to controlling the related variables constant from 2000-2018 (Supplementary Figs. 11-12). In addition, we estimated the contributions of CO_2 fertilization and climate change to the trend in absolute $\delta DOY_{GPP, LAI}$ based on the model outputs from the TRENDY S0-S2 simulations (Supplementary Figs. 14-15).

510

Data availability

The CSIF data set is from https://doi.org/10.17605/OSF.IO/8XQY6, the GOME-2 SIF data set is from https://avdc.gsfc.nasa.gov/pub/data/satellite/MetOp/GOME_F/, the MODIS NDVI data set is from https://lpdaac.usgs.gov/products/mod13c1v006/, the reprocessed LAI data set is from http://globalchange.bnu.edu.cn/research/laiv6, the FLUXNET2015 data set is from https://fluxnet.org/data/fluxnet2015-dataset/, the surface air temperature and shortwave radiation data sets are from https://vesg.ipsl.upmc.fr/thredds/catalog/work/p529viov/cruncep/V9_1901_2017/catalog.html, the soil-water content data set is from https://disc.gsfc.nasa.gov/datasets/GLDAS_NOAH025_3H_2.1/summary?keywords=

521   GLDAS, the SLA, Nm, and Pm data sets are from

522   https://github.com/abhirupdatta/global_maps_of_plant_traits, the canopy height and

523   maximum rooting depth data sets are from

524   https://webmap.ornl.gov/ogc/dataset.jsp?dg_id=10023_1   and

525   https://wci.earth2observe.eu/thredds/catalog/usc/root-depth/catalog.html, the ASR and

526   plant species data sets are from https://ecotope.org/anthromes/biodiversity/plants/data/

527   and https://databasin.org/datasets/43478f840ac84173979b22631c2ed672/ and the tree

528   density data set is from https://elischolar.library.yale.edu/yale_fes_data/1/.

529

530   **References**

531   1   Piao, S., Friedlingstein, P., Ciais, P., Viovy, N. & Demarty, J. Growing season extension

532   and its impact on terrestrial carbon cycle in the Northern Hemisphere over the past 2

533   decades. *Global Biogeochemical Cycles* **21**, GB3018 (2007).

534   2   Richardson, A. D. *et al.* Climate change, phenology, and phenological control of

535   vegetation feedbacks to the climate system. *Agr Forest Meteorol* **169**, 156-173 (2013).

536   3   Xia, J., Niu, S., Ciais, P. & Janssens, I. A. Joint control of terrestrial gross primary

537   productivity by plant phenology and physiology. *Proceedings of the National Academy*

538   *of Sciences* **112**, 2788-2793 (2015).

539   4   Yang, J. *et al.* Divergent shifts in peak photosynthesis timing of temperate and alpine

540   grasslands in China. *Remote Sensing of Environment* **233**, 111395 (2019).

541   5   Medlyn & B., E. Physiological basis of the light use efficiency model. *Tree Physiology*

542   **18**, 167 (1998).

543   6   Turner, D. P., Urbanski, S., Bremer, D., Wofsy, S. C. & Gregory, M. A cross-biome

544   comparison of daily light use efficiency for gross primary production. *Global Change*

545   *Biology* **9**, 383-395 (2003).

546   7   Monteith, J. L. Solar Radiation and Productivity in Tropical Ecosystems. *J. Appl. Ecol.*

547   **9**, 747-766 (1972).

548   8   Wang, H. *et al.* Towards a universal model for carbon dioxide uptake by plants. *Nat*

549   *Plants* **3**, 734-741 (2017).

550   9   Wang, X. *et al.* Globally Consistent Patterns of Asynchrony in Vegetation Phenology

551   Derived From Optical, Microwave, and Fluorescence Satellite Data. *Journal of*

552   *Geophysical Research: Biogeosciences* **125** (2020).

553   10   Huang, K., Xia, J., Wang, Y. & Ahlstrom, A. Enhanced peak growth of global vegetation

554   and its key mechanisms. *Nature Ecology & Evolution* **2**, 1897-1905 (2018).

555   11   Xu, C., Liu, H., Williams, A. P., Yin, Y. & Wu, X. Trends toward an earlier peak of the

556   growing season in Northern Hemisphere mid-latitudes. *Global Change Biology* **22**,

557   2852-2860 (2016).

558   12   Park, T., Chen, C. & Macias-Fauria, M. Changes in timing of seasonal peak

559   photosynthetic activity in northern ecosystems. *Global Change Biology* **25**, 2382-2395

560   (2019).

561   13   Poorter, H. *et al.* Biomass allocation to leaves, stems and roots: meta-analyses of

562   interspecific variation and environmental control. *New Phytologist* **193**, 30-50 (2012).

563   14   Zhang, Y., Joiner, J., Alemohammad, S. H., Zhou, S. & Gentine, P. A global spatially

564   contiguous solar-induced fluorescence (CSIF) dataset using neural networks.

565   *Biogeosciences* **15**, 5779-5800 (2018).

566   15   Frankenberg, C. *et al.* New global observations of the terrestrial carbon cycle from

567   GOSAT: Patterns of plant fluorescence with gross primary productivity. *Geophysical*

568   *Research Letters* **38**, n/a-n/a (2011).

569   16   Yuan, H., Dai, Y., Xiao, Z., Ji, D. & Shangguan, W. Reprocessing the MODIS Leaf Area

570   Index products for land surface and climate modelling. *Remote Sensing of Environment*

571   **115**, 1171-1187 (2011).

572   17   Elith, J., Leathwick, J. R. & Hastie, T. A working guide to boosted regression trees. *J.*

573   *Anim. Ecol.* **77**, 802-813 (2008).

574   18   Wang, X. *et al.* Globally Consistent Patterns of Asynchrony in Vegetation Phenology

575   Derived From Optical, Microwave, and Fluorescence Satellite Data.   **125**,

576   e2020JG005732 (2020).

577   19   Zhang, Y., Commane, R., Zhou, S., Williams, A. P. & Gentine, P. Light limitation

578   regulates the response of autumn terrestrial carbon uptake to warming. *Nature Climate*

579   *Change* **10**, 739-743 (2020).

580   20   Yuan, W. *et al.* Global comparison of light use efficiency models for simulating

581   terrestrial vegetation gross primary production based on the LaThuile database.

582   *Agricultural and Forest Meteorology* **192-193**, 108-120 (2014).

583   21   Reich, P. B. *et al.* Temperature drives global patterns in forest biomass distribution in

584   leaves, stems, and roots. *Proceedings of the National Academy of Sciences* **111**,

585   13721-13726 (2014).

586   22   Wright, I. J., Reich, P. B. & Westoby, M. The worldwide leaf economics spectrum.

587   *Nature* **428**, 821-827 (2004).

588   23   Reich, P. B., Oleksyn, J. & Wright, I. J. Leaf phosphorus influences the photosynthesis–

589   nitrogen relation: a cross-biome analysis of 314 species.   (2009).

590   24   Chen, Y., Han, W., Tang, L., Tang, Z. & Fang, J. Leaf nitrogen and phosphorus

591   concentrations of woody plants differ in responses to climate, soil and plant growth

592   form. *Ecography* **36**, 178-184 (2013).

593   25   Jiang, M., Caldararu, S., Zaehle, S., Ellsworth, D. S. & Medlyn, B. E. Towards a more

594   physiological representation of vegetation phosphorus processes in land surface

595   models. *New Phytologist* **222**, 1223-1229 (2019).

596   26   Kergoat, L., Lafont, S., Arneth, A., Le Dantec, V. & Saugier, B. Nitrogen controls plant

597   canopy light-use efficiency in temperate and boreal ecosystems. *Journal of*

598   *Geophysical Research: Biogeosciences* **113** (2008).

599   27   Du, E. *et al.* Global patterns of terrestrial nitrogen and phosphorus limitation. *Nature*

600   *Geoscience* **13**, 221-226 (2020).

601   28   Cleveland, C. C. *et al.* Patterns of new versus recycled primary production in the

602   terrestrial biosphere. *Proceedings of the National Academy of Sciences* **110**, 12733-

603   12737 (2013).

604   29   Veneklaas, E. J. *et al.* Opportunities for improving phosphorus-use efficiency in crop

605   plants. *New Phytologist* **195**, 306-320 (2012).

606   30   Janssens, I. A. & Luyssaert, S. Nitrogen's carbon bonus. *Nature Geoscience* **2**, 318-

607   319 (2009).

608   31   Luo, X. *et al.* Global variation in the fraction of leaf nitrogen allocated to photosynthesis.

609   *Nature Communications* **12**, 4866 (2021).

610   32   Lambers, H., Iii, F. & Pons, T. L. *Plant physiological ecology: Second edition*. (Plant

611   physiological ecology: Second edition, 2008).

612   33   Vose, J. M. *et al.* Factors Influencing the Amount and Distribution of Leaf Area of Pine

613   Stands. *Ecol Bull*, 102-114 (1994).

614   34   Carter, S. K., Saenz, D. & Rudolf, V. H. W. Shifts in phenological distributions reshape

615   interaction potential in natural communities. *Ecol Lett* **21**, 1143-1151 (2018).

616   35   Sitch, S. *et al.* Recent trends and drivers of regional sources and sinks of carbon

617   dioxide. *Biogeosciences* **12**, 653-679 (2015).

618   36   Farquhar, G. D., von Caemmerer, S. & Berry, J. A. A biochemical model of

619   photosynthetic CO_2 assimilation in leaves of C3 species. *Planta* **149**, 78-90 (1980).

620   37   Krinner, G. *et al.* A dynamic global vegetation model for studies of the coupled

621   atmosphere-biosphere system. *Global Biogeochemical Cycles* **19** (2005).

622   38   Murray-Tortarolo, G. *et al.* Evaluation of Land Surface Models in Reproducing Satellite-

623   Derived LAI over the High-Latitude Northern Hemisphere. Part I: Uncoupled DGVMs.

624   *Remote Sensing* **5**, 4819-4838 (2013).

625   39   Lawrence, D. M., Fisher, R. A. & Koven, C. D. The Community Land Model Version 5:

626   Description of New Features, Benchmarking, and Impact of Forcing Uncertainty.

627   *Journal of Advances in Modeling Earth Systems* **11**, 4245-4287 (2019).

628   40   Goll, D. S., Winkler, A. J. & Raddatz, T. Carbon–nitrogen interactions in idealized

629   simulations with JSBACH (version 3.10). *Geoscientific Model Development* **10**, 2009-

630   2030 (2017).

631   41   Goll, D. S., Vuichard, N. & Maignan, F. A representation of the phosphorus cycle for

632   ORCHIDEE (revision 4520). *Geoscientific Model Development* **10**, 3745-3770 (2017).

633   42   Sun, Y., Goll, D. S. & Chang, J. Global evaluation of the nutrient-enabled version of the

634   land surface model ORCHIDEE-CNP v1.2 (r5986). *Geoscientific Model Development*

635   **14**, 1987-2010 (2021).

636   43   Clark, D. B., Mercado, L. M. & Sitch, S. The Joint UK Land Environment Simulator

637   (JULES), model description – Part 2: Carbon fluxes and vegetation dynamics.

638   *Geoscientific Model Development* **4**, 701-722 (2011).

639   44   Terrer, C. *et al.* Nitrogen and phosphorus constrain the CO2 fertilization of global plant

640   biomass. *Nature Climate Change* **9**, 684-689 (2019).

641   45   Reyes-Fox, M. *et al.* Elevated CO2 further lengthens growing season under warming

642   conditions. *Nature* **510**, 259-262 (2014).

643   46   Guanter, L. *et al.* Global and time-resolved monitoring of crop photosynthesis with

644   chlorophyll fluorescence. *Proceedings of the National Academy of Sciences of the*

645   *United States of America* **111**, E1327-1333 (2014).

646   47   Sun, Y. *et al.* OCO-2 advances photosynthesis observation from space via solar-

647   induced chlorophyll fluorescence.   **358**, eaam5747 (2017).

648   48   Joiner, J. *et al.* The seasonal cycle of satellite chlorophyll fluorescence observations

649   and its relationship to vegetation phenology and ecosystem atmosphere carbon

650   exchange. *Remote Sensing of Environment* **152**, 375-391 (2014).

651   49   Chu, D. *et al.* Long time-series NDVI reconstruction in cloud-prone regions via spatio-

652   temporal tensor completion. *Remote Sensing of Environment* **264** (2021).

653   50   Joiner, J. *et al.* Global monitoring of terrestrial chlorophyll fluorescence from moderate-

654   spectral-resolution near-infrared satellite measurements: methodology, simulations,

655   and application to GOME-2. *Atmospheric Measurement Techniques* **6**, 2803-2823

656   (2013).

657   51   Zhang, Y., Joiner, J., Gentine, P. & Zhou, S. Reduced solar-induced chlorophyll

658   fluorescence from GOME-2 during Amazon drought caused by dataset artifacts. **24**,

659   2229-2230 (2018).

660   52   Rodell, M., Houser, P. R. & Jambor, U. The Global Land Data Assimilation System.

661   *Bulletin of the American Meteorological Society* **85**, 381-394 (2004).

662   53   Reichstein, M. *et al.* On the separation of net ecosystem exchange into assimilation

663   and ecosystem respiration: review and improved algorithm. **11**, 1424-1439 (2005).

664   54   LASSLOP, G. *et al.* Separation of net ecosystem exchange into assimilation and

665   respiration using a light response curve approach: critical issues and global evaluation.

666   **16**, 187-208 (2010).

667   55   Vautard, R., Yiou, P. & Ghil, M. Singular-spectrum analysis: A toolkit for short, noisy

668   chaotic signals. *Physica D: Nonlinear Phenomena* **58**, 95-126 (1992).

669   56   Zhou, S. *et al.* Dominant role of plant physiology in trend and variability of gross primary

670   productivity in North America. *Scientific Reports* **7**, 41366 (2017).

671   57   Butler, E. E., Datta, A. & Flores-Moreno. Mapping local and global variability in plant

672   trait distributions. *Proceedings of the National Academy of Sciences of the United*

673   *States of America* **114**, E10937-E10946 (2017).

674   58   Simard, M., Pinto, N., Fisher, J. B. & Baccini, A. Mapping forest canopy height globally

675   with spaceborne lidar. *Journal of Geophysical Research-Biogeosciences* **116** (2011).

676   59   Ellis, E. C., Antill, E. C. & Kreft, H. All Is Not Loss: Plant Biodiversity in the

677   Anthropocene. *PLoS ONE* **7**, e30535- (2012).

678   60   Kier, G., Mutke, J., Dinerstein, E., Ricketts, T. H. & Barthlott, W. Global patterns of plant

679   diversity and floristic knowledge. *J. Biogeogr.* **32**, 1107-1116 (2005).

680   61   Running, S. W., Thornton, P. E., Nemani, R. & Glassy, J. M.   44-57 (Springer

681   New York, 2000).

682

688

689 **Author contributions**

690 S.L.P. and Z.C.Z. designed the study; Q.Z. performed the analysis; All authors

691 contributed to the interpretation of the results and the writing of the paper.

692

693 **Author Information**

694 Reprints and permissions information is available at www.nature.com/reprints. The

695 authors have no competing financial interests. Correspondence and requests for

696 materials should be addressed to Z.C.Z. (zhu.zaichun@pku.edu.cn) or S.L.P.

697   (slpiao@pku.edu.cn).

698

699   **Figure Legends**

700   **Figure 1 | Timing of seasonal peak photosynthesis, canopy structure, and climatic**

701   **variables. a**, Probability densities of DOY_{CSIF}, DOY_{NDVI}, DOY_{SWC}, DOY_{Rad}, and

702   DOY_{TEMP}. The colors and dotted lines indicate their averages weighted by area and

703   CSIF value at the pixel level. **b**, Spatial patterns of DOY_{SWC}, DOY_{Rad}, DOY_{TEMP},

704   DOY_{CSIF}, and DOY_{NDVI} in northern ecosystems. The legend shows the month DOY

705   belonging to, with a and b indicating the first and second half of the month.

706

707   **Figure 2 | Comparison between the timing of seasonal peak photosynthesis and**

708   **canopy structure in northern ecosystems. a**, Spatial pattern of the relationship of

709   seasonal peak timing between photosynthesis and canopy structure represented by

710      $\delta DOY_{CSIF, NDVI}$ (DOY_{CSIF} - DOY_{NDVI}). **b**, Climatic constraints of temperature (blue) and

711   soil-water content (orange) on vegetation photosynthesis in northern ecosystems,

712   represented by $\delta DOY_{CSIF, TEMP}$ ($DOY_{CSIF} - DOY_{TEMP}$) and $\delta DOY_{CSIF, SWC}$ ($DOY_{CSIF} -$

713   DOY_{SWC}) respectively.

714

715   **Figure 3 | Factors accounting for the mismatch in seasonal peak timing between**

716   **photosynthesis and canopy structure. a**, Relative contribution of 18 factors

717   influencing the spatial variation of negative $\delta DOY_{CSIF, NDVI}$ evaluated by BRT models

718   based on four ecosystems: northern ecosystems, forests, shrublands, and grasslands.

The color scales represent different categories of factors: variables of climatic

conditions (TEMP, Tdr, SWC, and Rad; dark blue); variables of climatic synergy

(r(TEMP, SWC), $\delta DOY_{CSIF, TEMP}$, $\delta DOY_{CSIF, SWC}$, and $\delta DOY_{CSIF, Rad}$; light blue); foliar

economic traits (Nm, Pm, NPr, and SLA; green); hydraulic traits (rooting depth and

canopy height, yellow); variables of biodiversity (ASR and Species, red); and others

(GSL and tree density, gray) (see Methods). **b,** Statistics for the cumulative contribution

of the factors from the same category. The colors of the donut chart correspond to the

color scale in **a**.

Figure 4 | Relationship between potential increase of GPP$_{max}$ (δGPP$_{max}$) and the

synchrony of peak timings between canopy structure and photosynthesis

(δDOY$_{GPP, NDVI}$) at 52 flux-tower sites. Each dot represents a site. The color scale

indicates the differences in seasonal peak timings between canopy structure and

environmental resources (δDOY_{NDVI}). The solid gray line indicates a linear regression

fit, and the dashed lines represent the 95% confidence interval.

Figure 5 | Timing of seasonal peak photosynthesis and canopy structure in

northern ecosystems simulated by the 14 TRENDY models. a, Comparison of

modeled DOY$_{LAI}$ and δDOY$_{GPP, LAI}$ with observed DOY$_{NDVI}$ and δDOY$_{CSIF, NDVI}$. The

colored dots indicate means. The vertical and horizontal error bars represent 0.5

standard deviations for DOY$_{LAI}$ and δDOY$_{GPP, LAI}$. The numerical labels indicate

different strategies of allocation of photosynthetic carbon: (1) only considering an

741 allometric relationship, (2) only considering resource limitation, and (3) considering

742 both. The gray shading represents the range of observations composed of means (solid

743 lines) and 0.5 standard deviations (dotted lines) for DOY_{NDVI} and $\delta DOY_{CSIF, NDVI}$. **b**,

744 Same as **a**, but for DOY_{GPP} and $\delta DOY_{GPP, LAI}$.

745

746 **Figure 6 | Changes in the mismatch in seasonal peak timing between**

747 **photosynthesis and canopy structure. a**, Interannual changes in observed absolute

748 $\delta DOY_{CSIF, NDVI}$ (black lines) and simulated absolute $\delta DOY_{GPP, LAI}$ (green lines) by

749 averaging 14 TRENDY models. The solid lines with markers and dotted lines indicate

750 annual mismatched days and regression lines. The trend is calculated by the Theil-Sen

751 estimator and tested with the Mann-Kendall test. Double asterisks indicate $p < 0.001$.

752 The shaded area shows the uncertainty range of models represented by half of the

753 standard deviation of the trends. **b** and **c**, Spatial patterns of trends in $\delta DOY_{CSIF, NDVI}$

754 during 2000-2018 and $\delta DOY_{GPP, LAI}$ during 2000-2017.
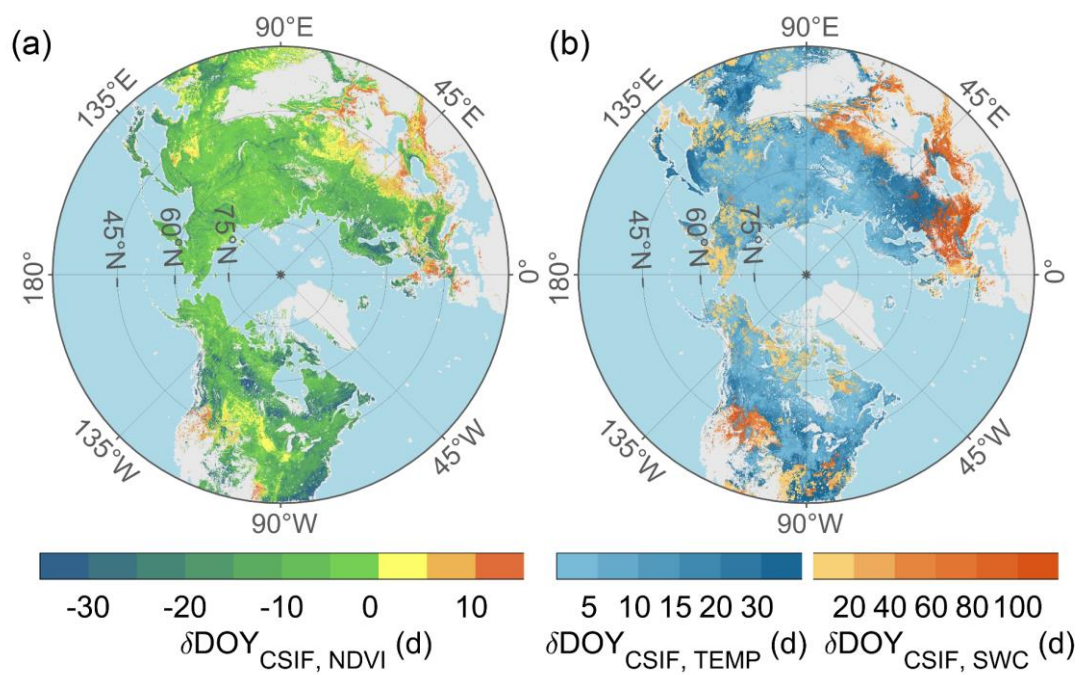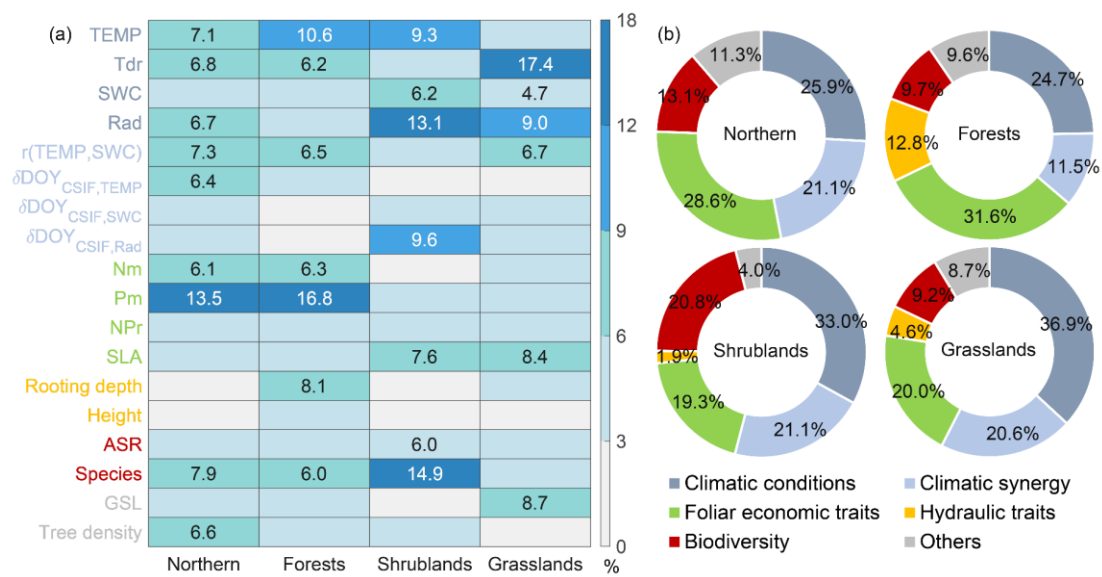
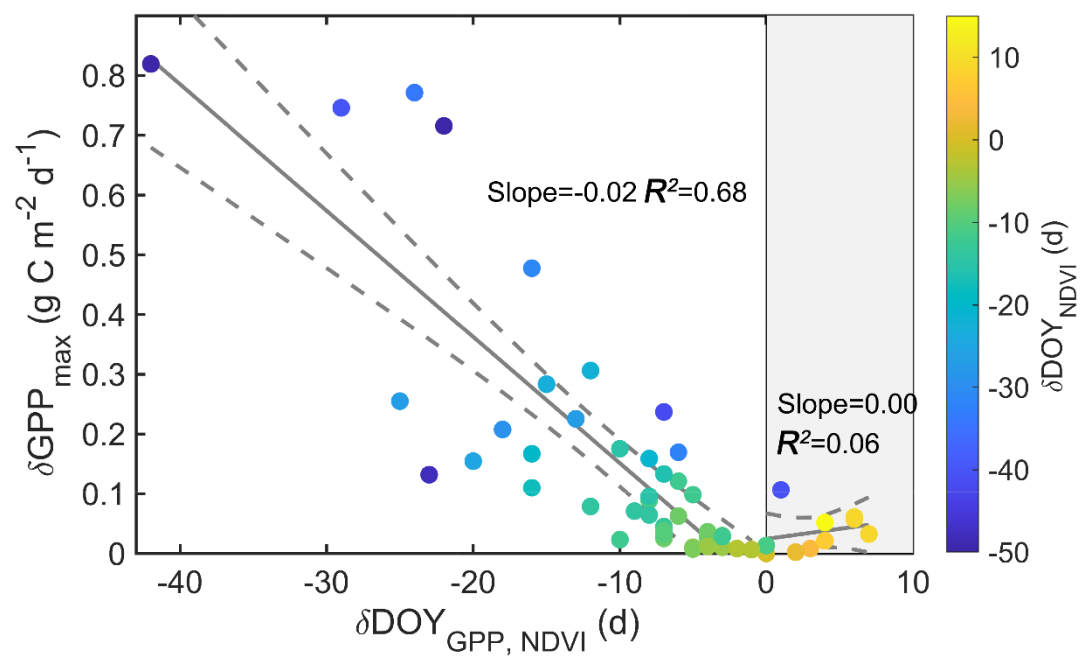755

756

Figure 1

760 **Figure 2**

761
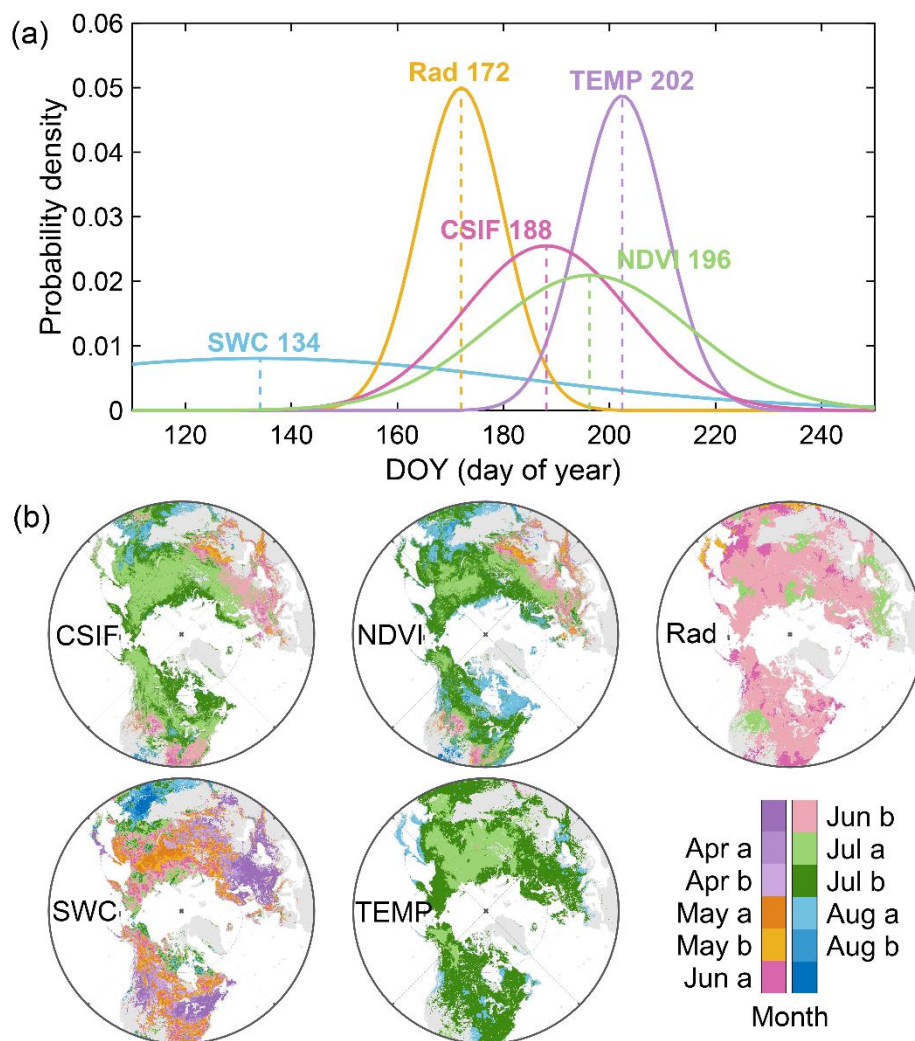
762

763   **Figure 3**

764

765

766 **Figure 4**
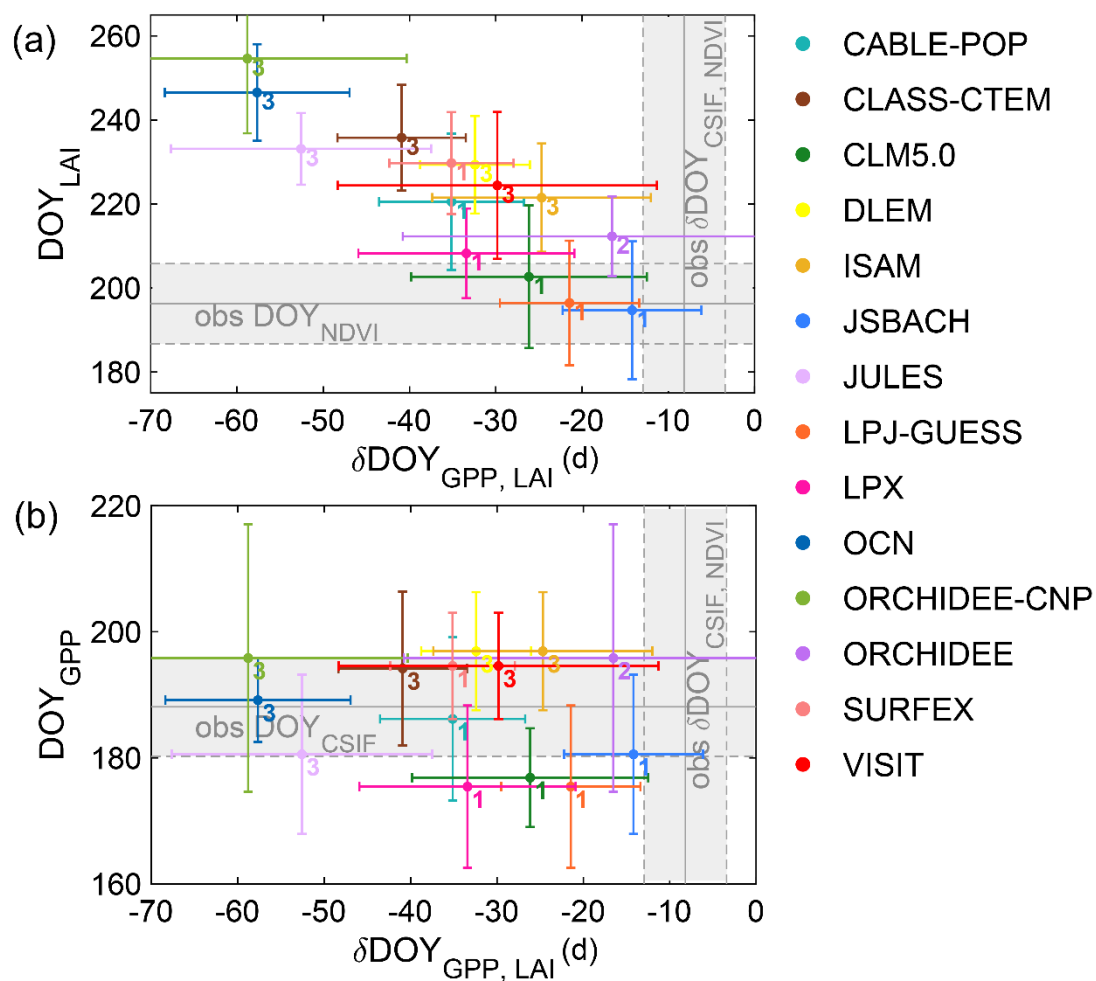

767

768

769   **Figure 5**

Figure 6

(a)

Observed: 0.39 ** d dec^{-1} TRENDY: 0.32 ± 0.48 d dec^{-1}

(b)   (c)

Trend in absolute δDOY$_{CSIF, NDVI}$ (d dec^{-1})   Trend in absolute δDOY$_{GPP, LAI}$ (d dec^{-1})